Prestack reverse time migration of shot profiles

John T. Etgen

ABSTRACT

This paper presents a method for the migration of shot records. It is based upon previous work on the migration of stacked data. The method is a full depth migration allowing for velocity to vary laterally as well as vertically and has no dip limitations. Because two-way wave propagation is desired and the goal is to migrate primaries only, a matched impedance form of the scalar wave equation is used to suppress internal reflection (Baysal et. al., 1984). The method is implemented with high-order finite differences as discussed in the previous paper (Etgen, 1986). A synthetic example is shown demonstrating the method for a simple model with 2 reflectors. The method is applied to field data from the Gulf of Mexico in another example.

INTRODUCTION

Prestack migration is used to image reflection data when the simpler assumptions of a flat-layered earth with no lateral velocity variation are no longer valid. Migration of shot profiles is only one of several possible methods of migrating data before stack; however, shot profiles have the advantage of being the record of one physical experiment, no artifice is required to image them. Also, the migration of shot profiles is a very local process, errors are not spread out, but remain local to the image of one shot record. Furthermore, a large dataset can be migrated as easily as a small one since there is no need to hold more than one profile in core-memory at any time. Finally, there are no restrictions on the sampling of the shot axis, and you need to migrate only enough shots to provide a satisfactory image of the subsurface.

I choose to think of migration, both post and pre-stack in terms of waves physically propagating in time. So reverse time migration provides a natural way to handle these wavefields in a physically intuitive manner. The wavefield is simply returned to its reflection point in the subsurface; it's amplitude gives some information on the size of the reflection coefficient at that point.

PRESTACK REVERSE TIME MIGRATION

Concepts

This section will explain a method of prestack migration in terms of time reversed wave propagation. To illustrate the versatility of the method and its link to the simpler case of zero-offset migration I will briefly describe the reverse time migration of stacked data then extend the concept to prestack migration. Other descriptions of reverse time migration of stacked data can be found in (Kosloff et. al, 1983), (Whitmore, 1983), (Levin, 1984), and the preceding paper to this one (Etgen, 1986). Kosloff and Reshef also discuss the migration of shot gathers (1986),but there are some differences in their implementation compared to this paper. Other related discussions dealing with reverse time migration of VSP's are give in (McMechan et. al, 1986) and (Whitmore et. al, 1986).

The reverse time migration of stacked data can be thought of as taking the recorded zero-offset or exploding reflector experiment that a stacked section represents, and back propagating this wavefield into the earth until time equals zero, the time the "exploding reflectors" explode. This gives an accurate depth position of the reflecting interfaces as long as the wave propagation and the events on the stacked section conform to the exploding reflector model.

In the prestack case, the argument is very similar. However, there is no exploding reflector model that allows imaging of the wavefield by simply stopping at time equals zero. Instead, we desire to apply some imaging method at the time that the reflected wave is excited, which is not at time equals zero, nor is it the same time for different reflectors or even for different locations along the same reflector. Physically the reflected wave is excited at the time the primary wave from the shot impinges on some boundary in the earth. Therefore, we can back propagate the recorded wavefield in a velocity model (for now presumed to be the correct one) and image by measuring its amplitude when it is coincident with the primary shot wavefield. In other words, when at some time during the back propagation, the recorded wave occupies the same location in x, z as the shot wavefield a reflection occurred at that place at that specific time. In some sense, during the forward problem i.e. the data collection, The shot wavefield is "convolved" with the subsurface geology. So ideally we desire to deconvolve the recorded wavefield (the output) by the shot wavefield (the input) to obtain the subsurface reflector positions (the system function). Ideally this could be done by dividing the Fourier transforms of the two wavefields at each time step to make an image. However, there are two practical problems; the first is that there will be zeroes in the spectra of the wavefields causing zero-divide errors. The second problem arises only from the fact that the method works in the physical coordinates; the extra work of taking Fourier transforms would make an already costly process much more expensive. A practical and inexpensive alternative is to multiply the two wavefields together; i.e. build a zero-lag crosscorrelation. So for each time-step,

the imaging is accomplished by simply multiplying together the value of the shot wavefield and the recorded wavefield for each grid-point and adding the result to an image plane. There are some other imaging methods based on least-squares type criteria discussed in Zhiming Li's thesis (Li, 1986), but the crosscorrelation seems robust and preserves some measure of the amplitude of the reflected wave well enough.

Implementation

This section briefly outlines the implementation used to do prestack depth migration of shot profiles. It is very similar to the algorithm presented in the previous paper, with the appropriate changes to handle the wavefields from a shot profile.

The first step of the process is to forward propagate a shot wavefield from the shot point to out past all the reflecting horizons of interest; this occurs in forward time. The propagation is done using the equation (1) the *2-way non-reflecting wave equation* (Baysal et. al., 1984).

$$\frac{\partial^2 U}{\partial t^2} = v(x,z)\,[\frac{\partial}{\partial x}v(x,z)\,\frac{\partial U}{\partial x} + \frac{\partial}{\partial z}v(x,z)\frac{\partial U}{\partial z}] \tag{1}$$

The next step is to propagate the recorded wavefield back towards the positions of the reflectors also using the non-reflecting wave equation. Then when the recorded wavefield is at the same instant of time as the forward propagated shot, the shot wavefield is time reversed so further evolution in time will cause the shot to collapse back towards the shot point. Now for each time step, the shot wavefield is backward propagated and the recorded wavefield is also backpropagated at the same time level. At any instant in time, places where the shot wavefield and the recorded wavefield overlap are the locations of reflecting interfaces. Thus, the two wavefields are multiplied together and added to the result of previous time levels to extract the position of the reflectors. This all proceeds until time equals zero when all of the reflected waves have been backpropagated into the model and imaged by the collapsing shot. In all cases, a high-order finite-difference implementation of equation (1) is used to do the wave propagation.

Synthetic example

Figures 1 through 4 show the migration procedure in progress for a simple model with a flat reflector and a dipping reflector. The profile that was migrated was generated by a scalar wave equation modeling program. For the migration the same velocity model was used as for the forward modeling because the purpose of the figures is only to show the operation of the algorithm. Figure 5 shows the velocity model used. Figure 6 shows the input model shot record used for the reverse time migration.

For each sequence of figures, I displayed the shot wavefield as (a), the back-propagated recorded

wavefield as (b), and the image plane at the current time level as (c). Figure 1 shows the wavefields and the image at a time level greater than the reflection time for all but a very small amount of the flat reflector. Therefore, the image, 1(c), is still largely empty because the wavefields have not propagated all the way back to the position of the reflectors. Note in 1(a) that the shot wavefield is still beyond the reflecting interfaces, and in 1(b) the recorded wavefield has not yet returned to the reflecting interfaces. In 1(b) the stronger wavefront is going towards the flat interface and the weaker wavefront is going towards the dipping interface.

Figures 2 show the wavefields and image plane after backpropagation for another 100 milliseconds (an earlier time). At this point in time, about one-half of the flat interface has been imaged by the collapsing shot wavefield and half is still returning to its reflection point. Note that the parts of the back-propagated recorded wavefield 2(b) that have passed outside of the position of the shot wavefield 2(a) have been imaged, and the parts still inside of the position of the shot wavefield are not yet imaged.

Figures 3 show the wavefields and image plane after another 100 milliseconds of back-propagation. Now, the flat interface has been completely imaged in 3(c) while only parts of the dipping interface have been imaged. Note in 3(b) that the recorded wave from the flat interface continues to propagate down after it has been imaged. Physically this is unrealistic because the recorded wave did not exist below the interface. However, it is not bothersome because it will not contribute to the image, we can just ignore it. The low frequency "smear" above the right part of the flat reflector is an artifact of the non-reflecting wave equation. It is at approximately the critical angle when the non-reflecting wave equation breaks down and reflects. Overall, though there are no significant internal reflections from the wavefields passing through the interfaces in the velocity model for angles less than critical.

Figures 4 show the wavefields after a further 100 milliseconds of back-propagation. Now, both the dipping reflector and the flat reflector are fully imaged in 4(c). In 4(a), all of the area of the model outside of the collapsing shot has been imaged. The area inside the collapsing shot has not yet been imaged, but we know that there are no reflectors inside so the migration is complete; 4(c) is the final image. Note that the amplitude of the events in the final section are proportional to the amplitude of the reflected wavefield.

Field data results

The next set of figures shows the results of pre-stack reverse time migration applied to field data. This data is the same as used by Zhiming Li in his thesis and SEP-48 (Li, SEP-48, SEP-49) The profiles are from the Gulf of Mexico and were recorded with 240 traces. The shot to near-offset distance was 312.5 meters; the trace spacing was 12.5 meters and the shot interval was 25 meters. For the migration, only 102 traces were actually propagated back for each shot profile.

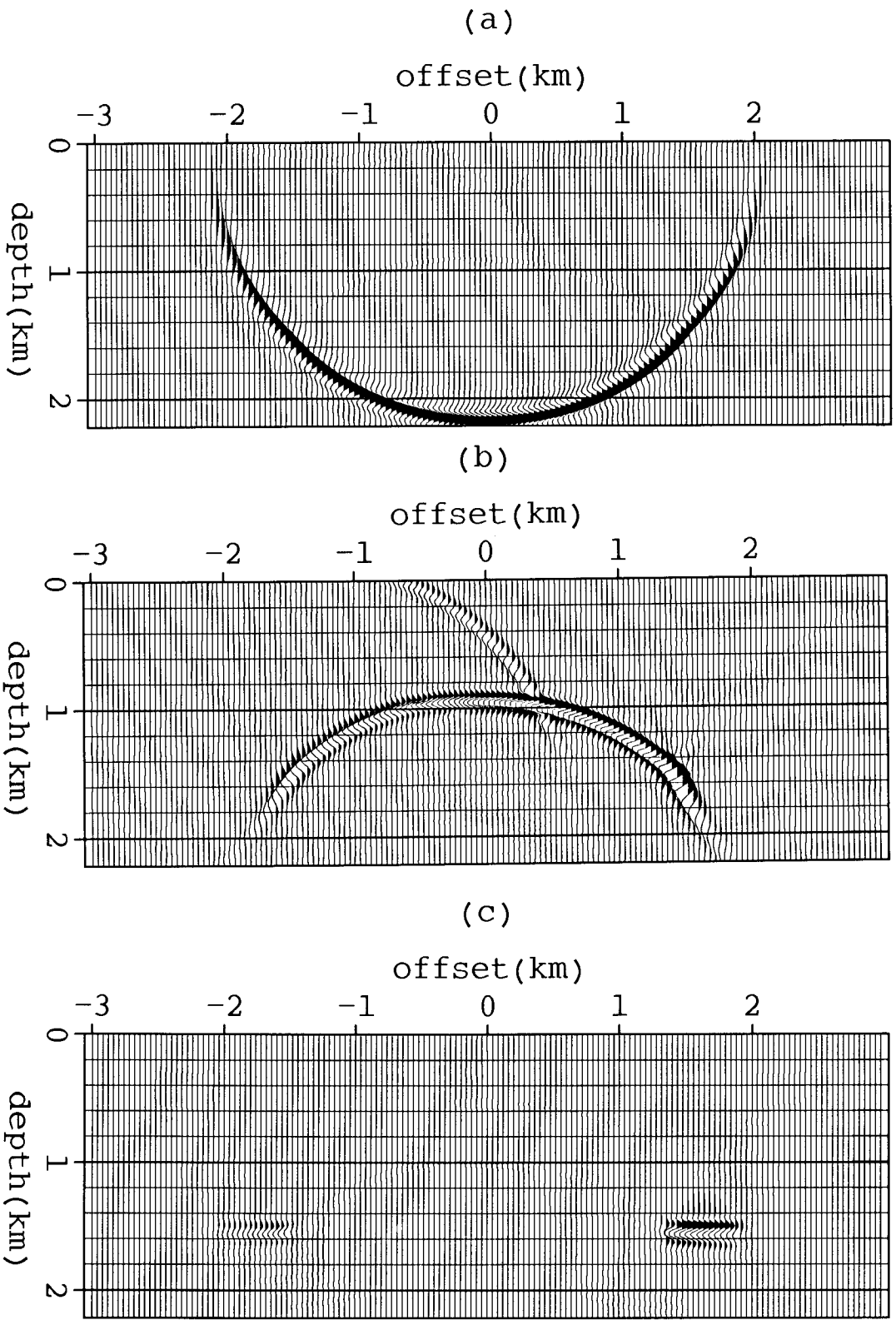

FIG. 1. (a) is the backward propagating shot wavefield; (b) is the backward propagating recorded wavefield;(c) is the image plane up through the current time level. Not much is imaged yet.

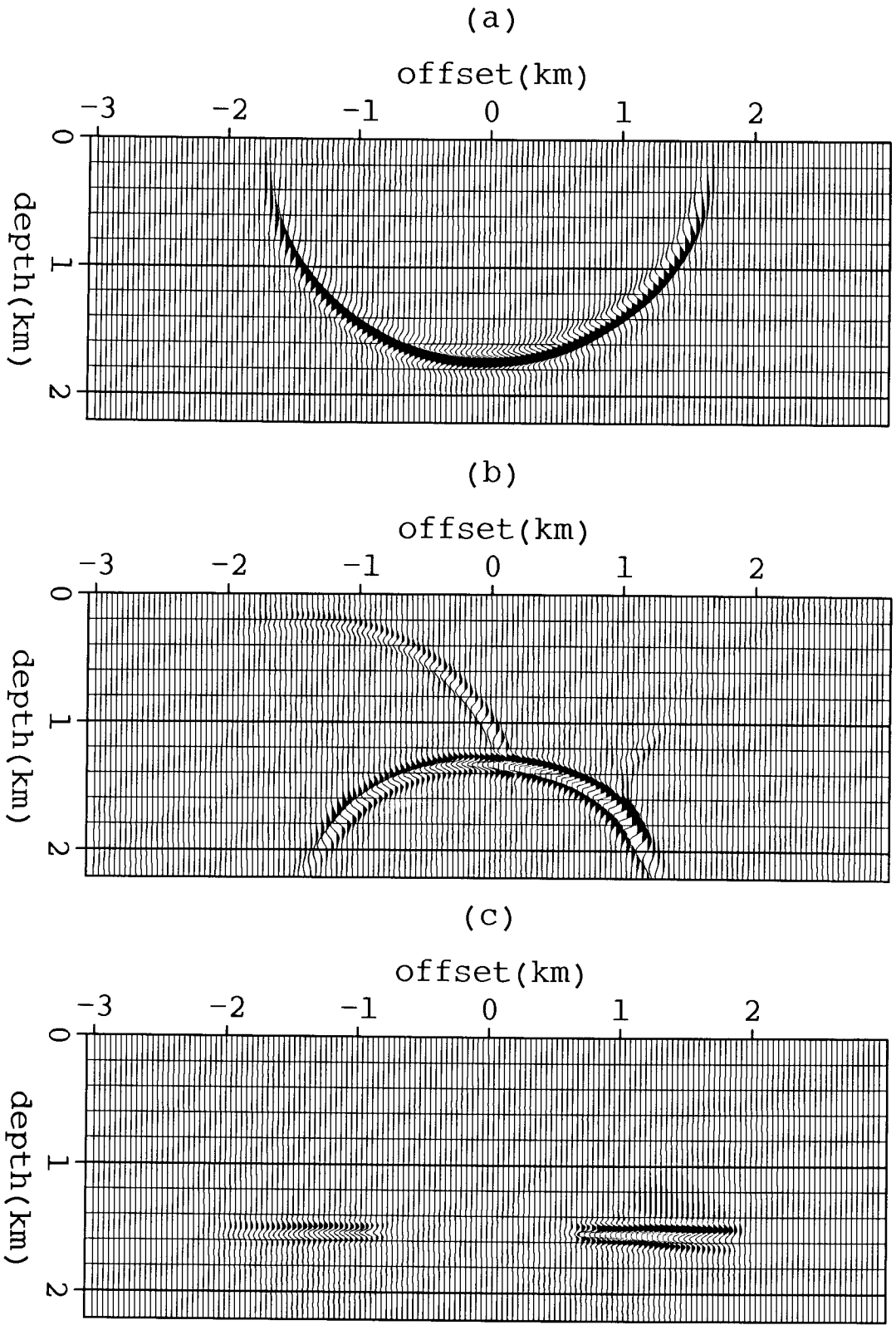

FIG. 2. (a) is the collapsing shot 100 ms. before Figure 1(a); (b) is the back-propagated reflected wavefield 100 ms. before 1(b); (c) is the updated image. The flat reflector is partially imaged.

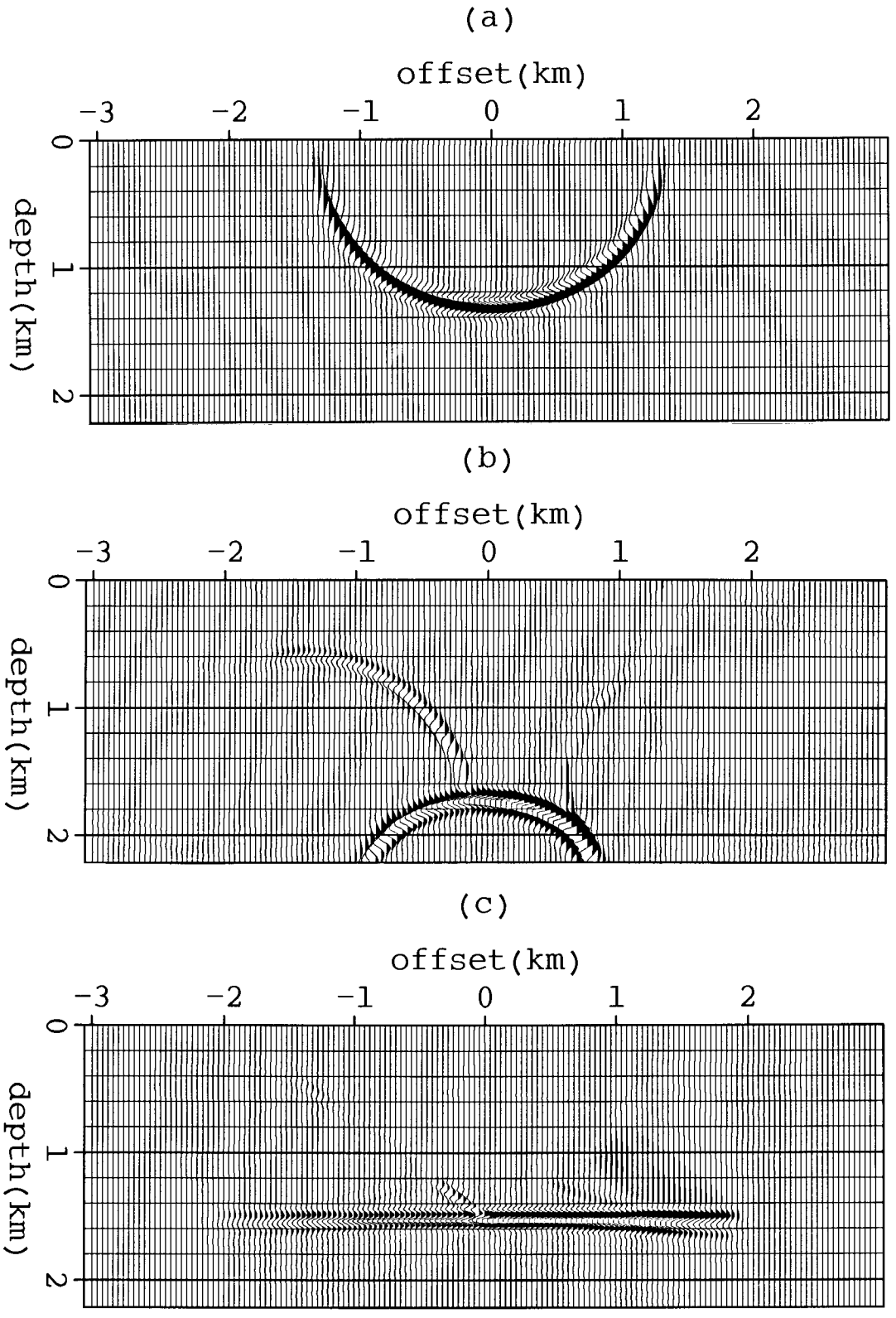

FIG. 3. (a) is the collapsing shot after another 100 ms backpropagation; (b) is the back-propagated reflected wavefield 100 ms. before 2(b); (c) is the updated image at this time level. The flat reflector is imaged, the dipping reflector is partially imaged. Remember time is running backwards!

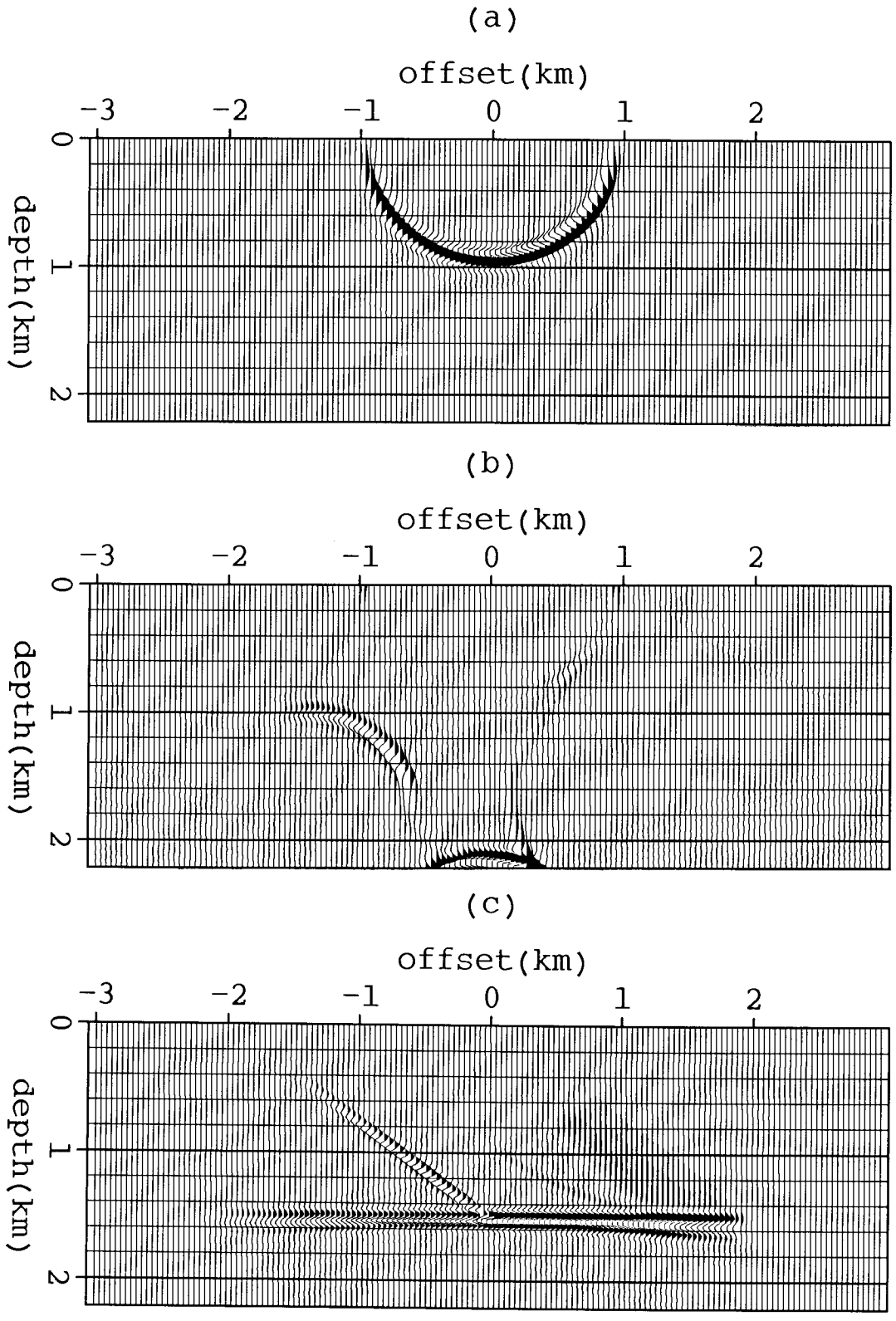

FIG. 4. (a) is the collapsing shot, now past all reflecting interfaces; (b) is the reflected wavefield also past the reflectors; (c) is the image that is now complete.

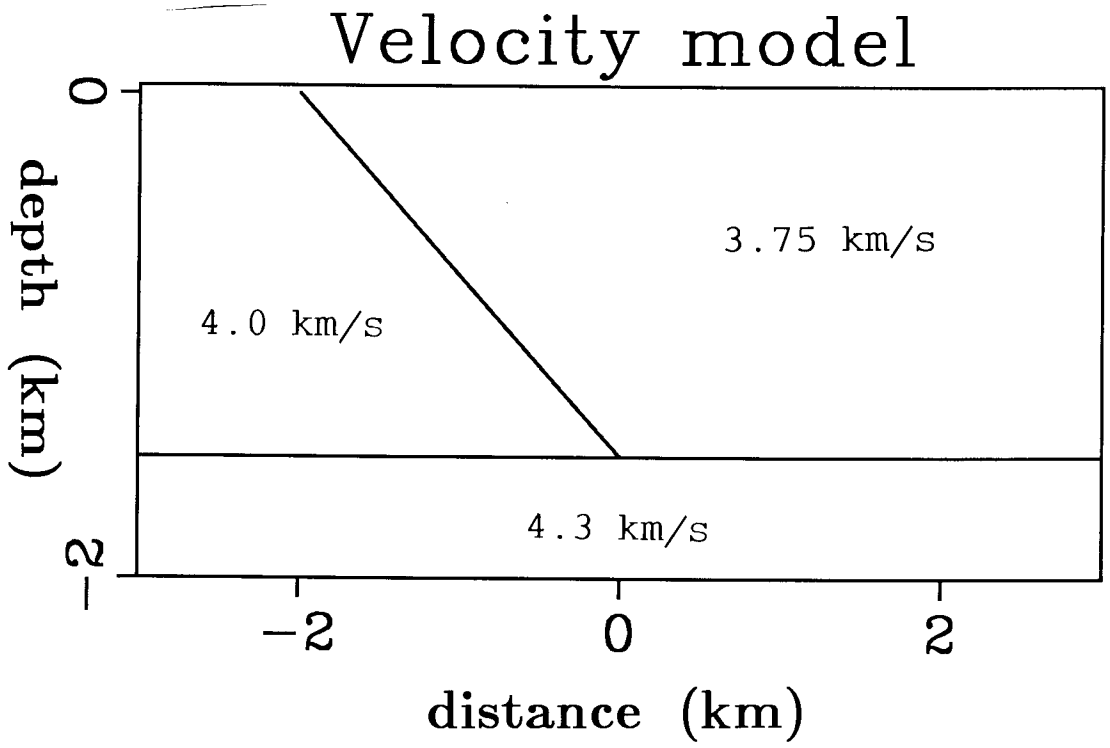

FIG. 5. Velocity model for synthetic example, Figure 1-4

The finite difference grid sizes for the velocity model was 12.5 meters in x by 12.5 meters in z and the time step size was 3 milliseconds. To facilitate stacking of the profiles and to remove the effects of boundary conditions, each profile was migrated in its correct location on a grid large enough to hold the image of all the profiles. Because the grid was so large, the computation time for the migration of 1 profile was approximately 11.5 CPU minutes. The grid was much larger than necessary for the migration of any individual profile so the number of grid points could have been reduced by more than a factor of 2 and all of the information would still be present in the image of each profile. This would cut the CPU time down to about 5.5 minutes per profile.

Figures 7 through 12 show six selected profiles that were migrated from this data set using reverse time migration. The high amplitude events are the partial images of the reflecting horizons. In particular note the various steeply-dipping fault-plane reflections "F" and the salt-sediment interface "S".

Truncation artifacts are visible as semicircular "smiles" coming from the edges of the reflector images. Most of the energy in the image comes from the subsurface area that was illuminated by the shot wavefield, while the truncation artifacts are small even though only 102 offsets are used in the migration and the nearest source-receiver offset is large (312.5 meters). Only at shallow depths do the artifacts have significant amplitude, and they will be suppressed in the

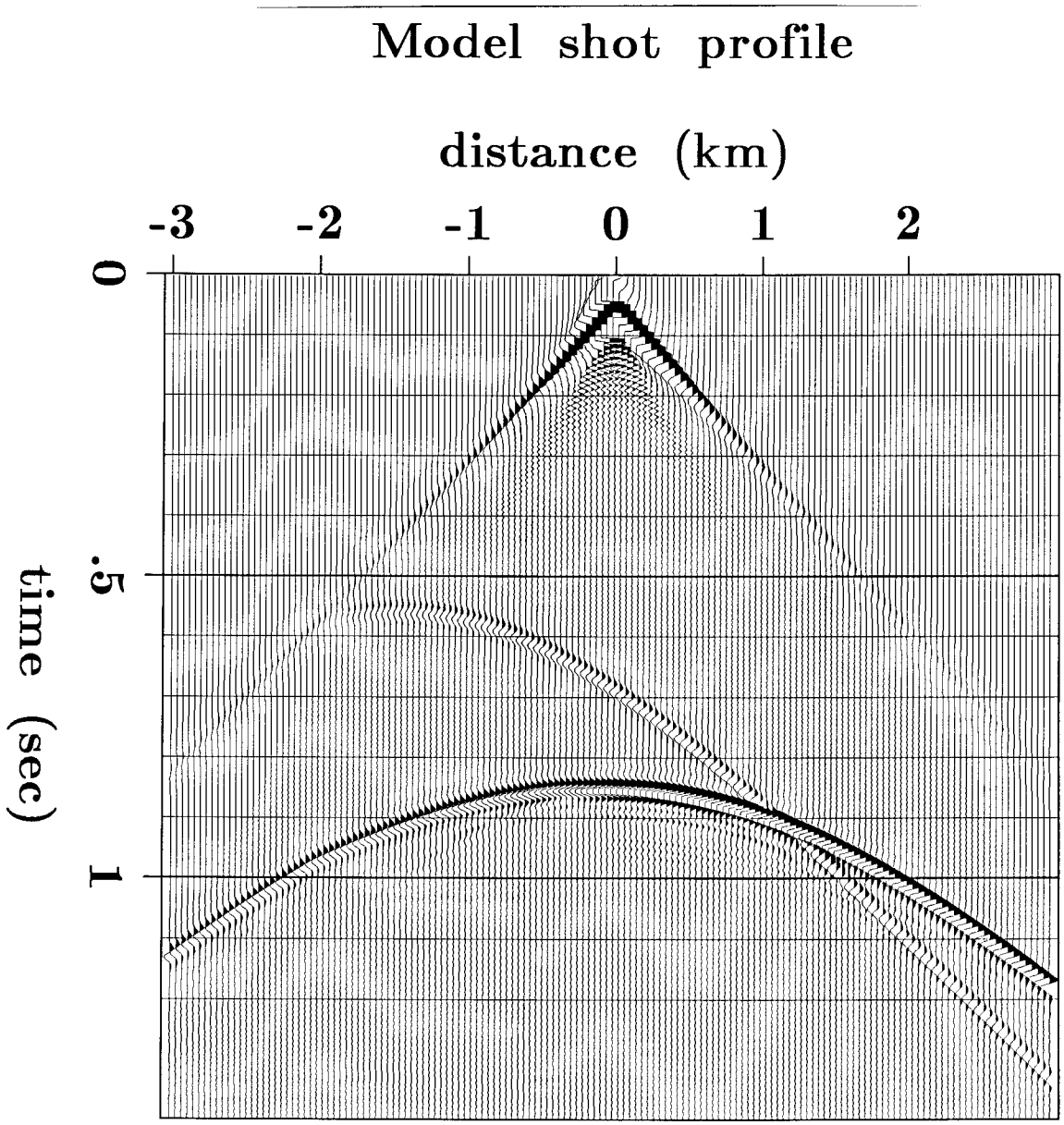

FIG. 6. Forward modeled field profile used for the synthetic migration example.

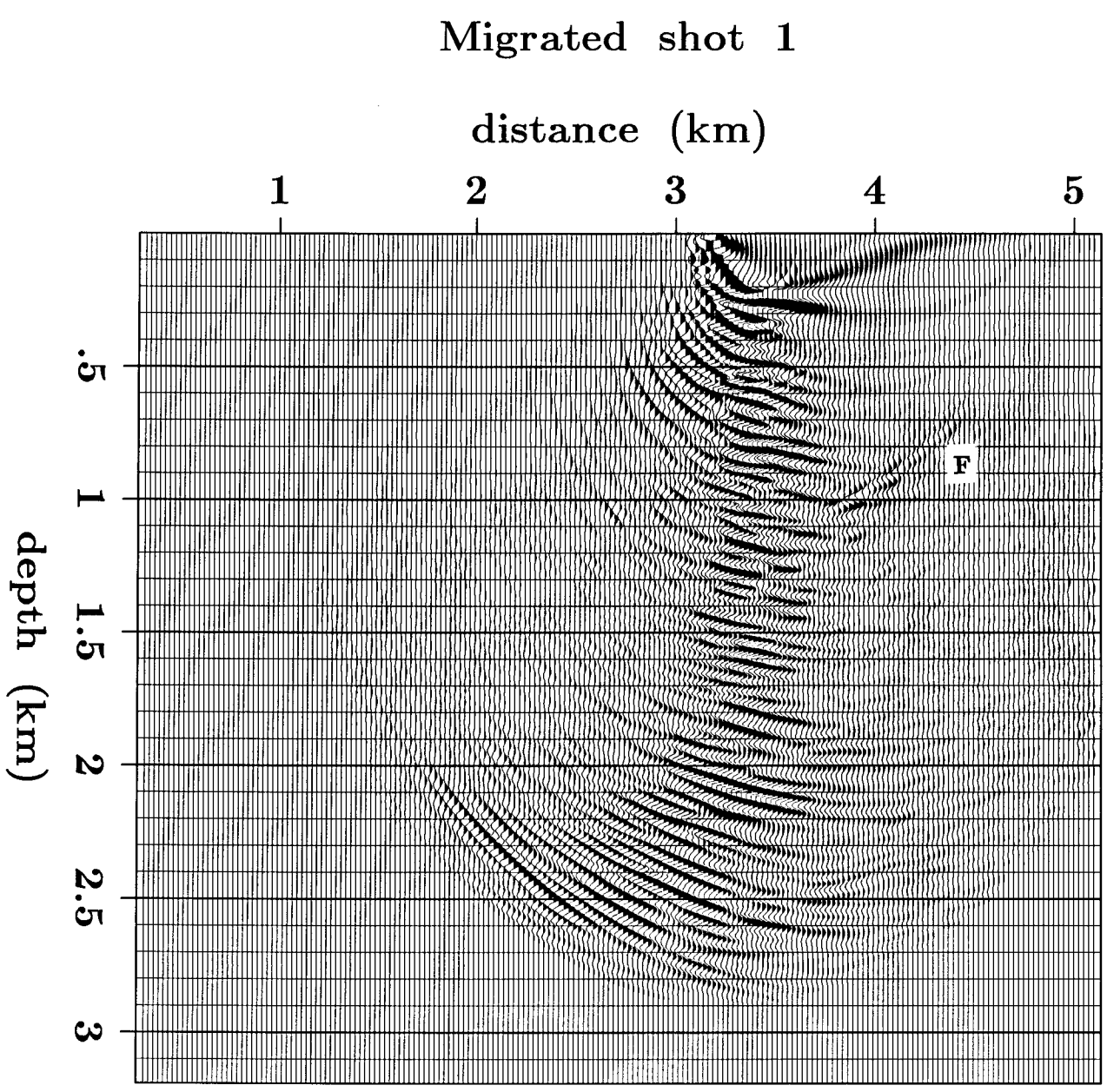

FIG. 7. Prestack migrated profile 1. Note fault-plane reflection "F".

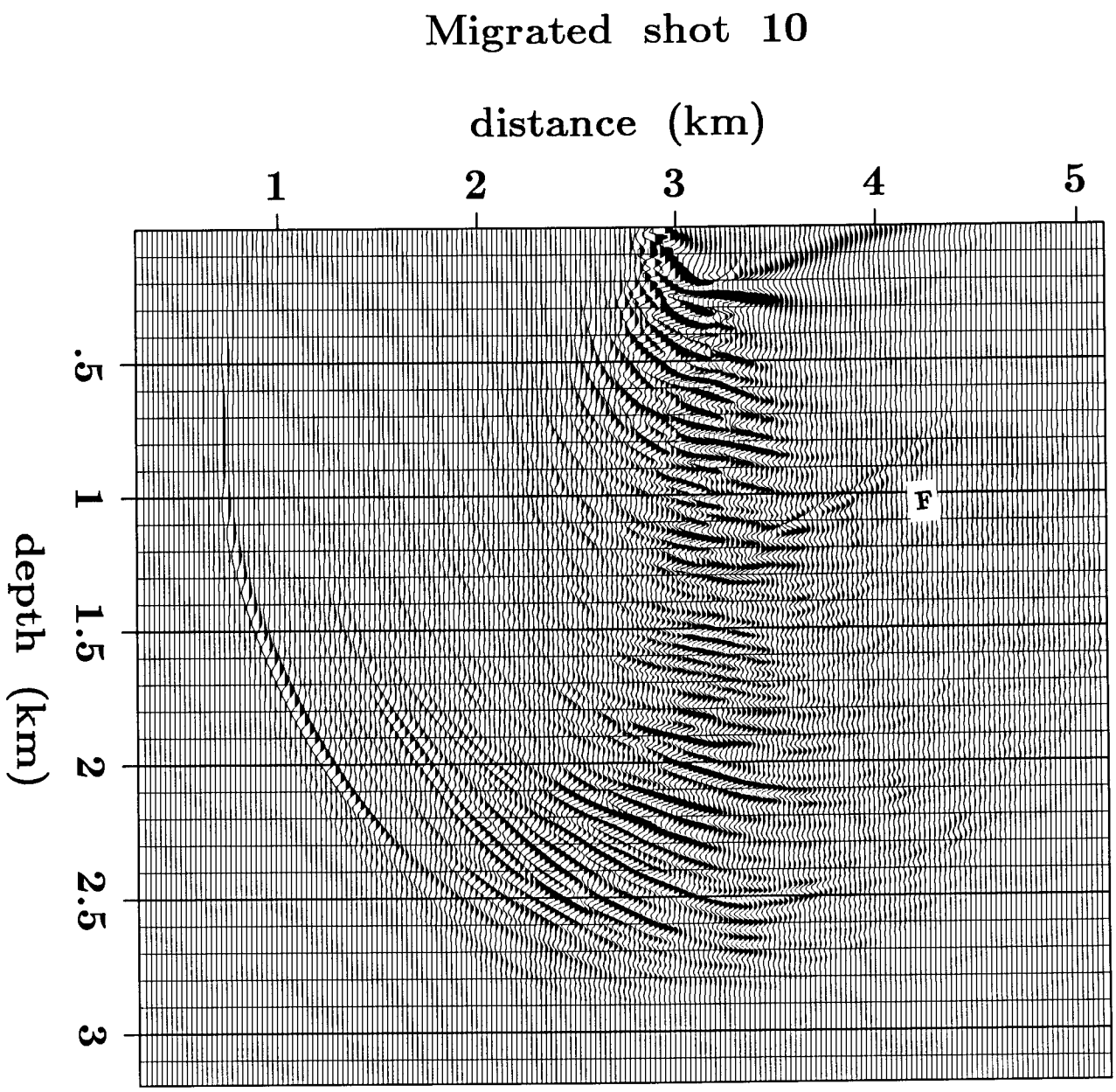

FIG. 8. Prestack migrated profile 10.

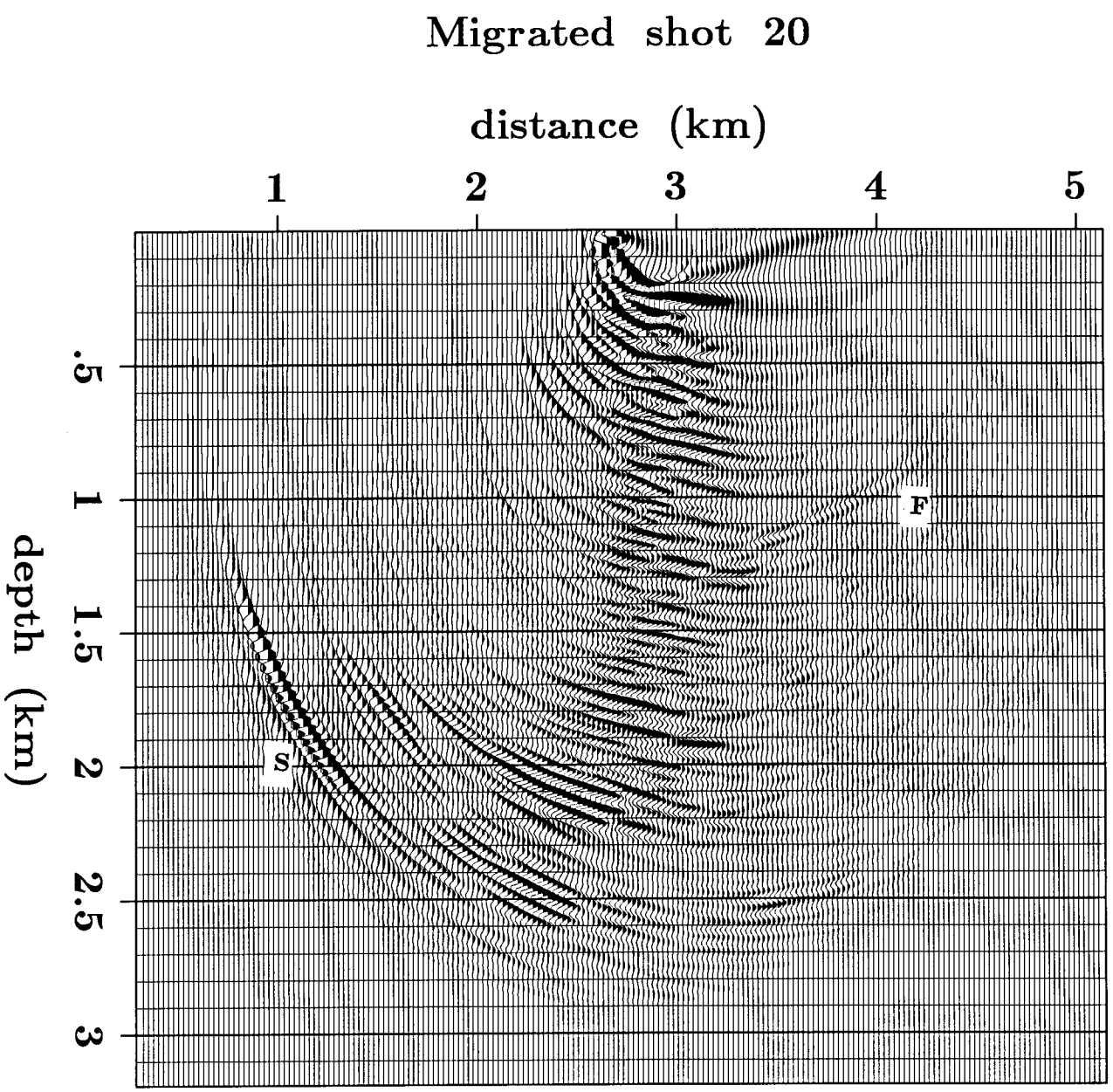

FIG. 9. Prestack migrated profile 20. Note fault-plane reflections "F" and salt-sediment interface reflection "S".

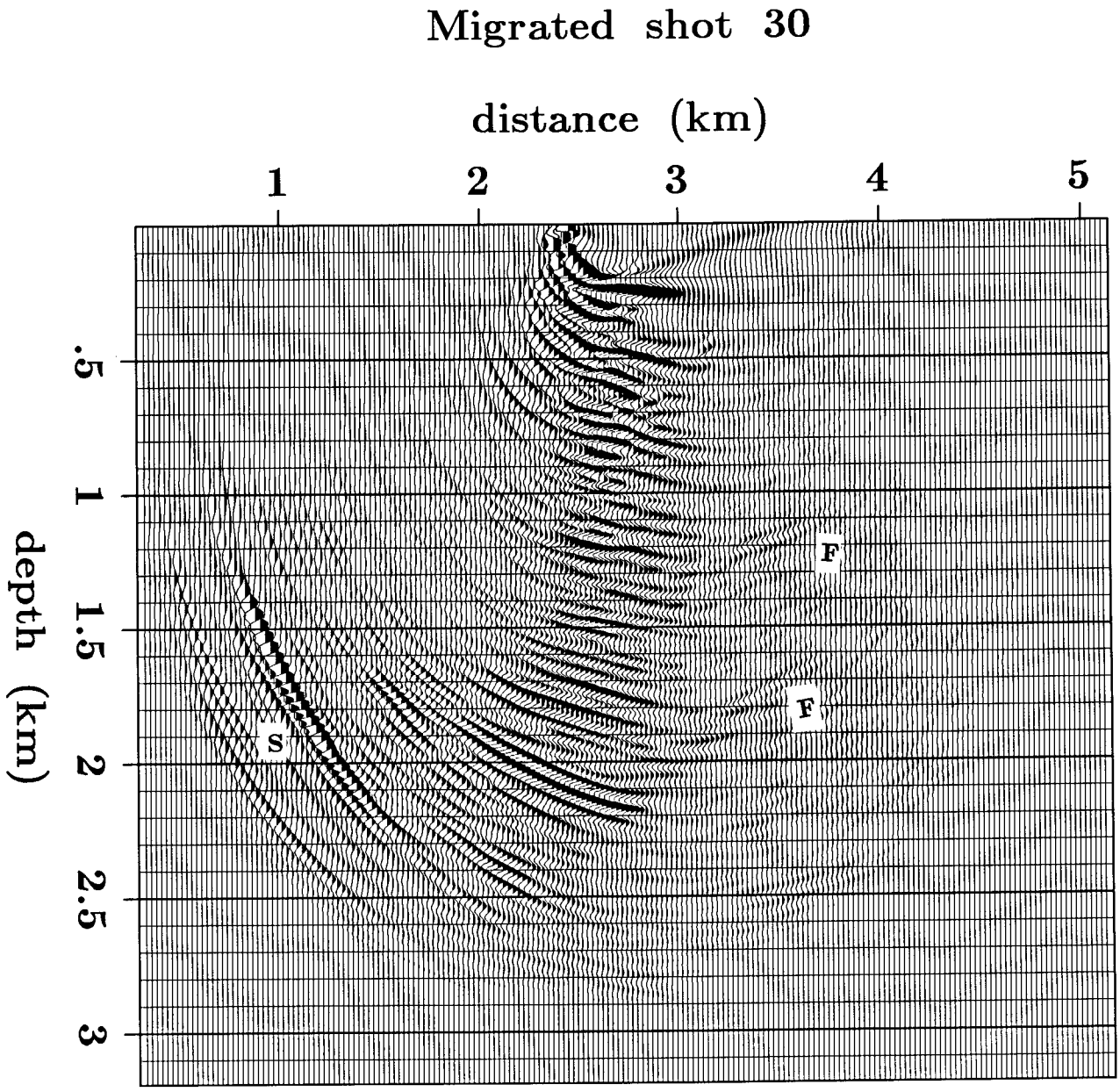

FIG. 10. Prestack migrated profile 30

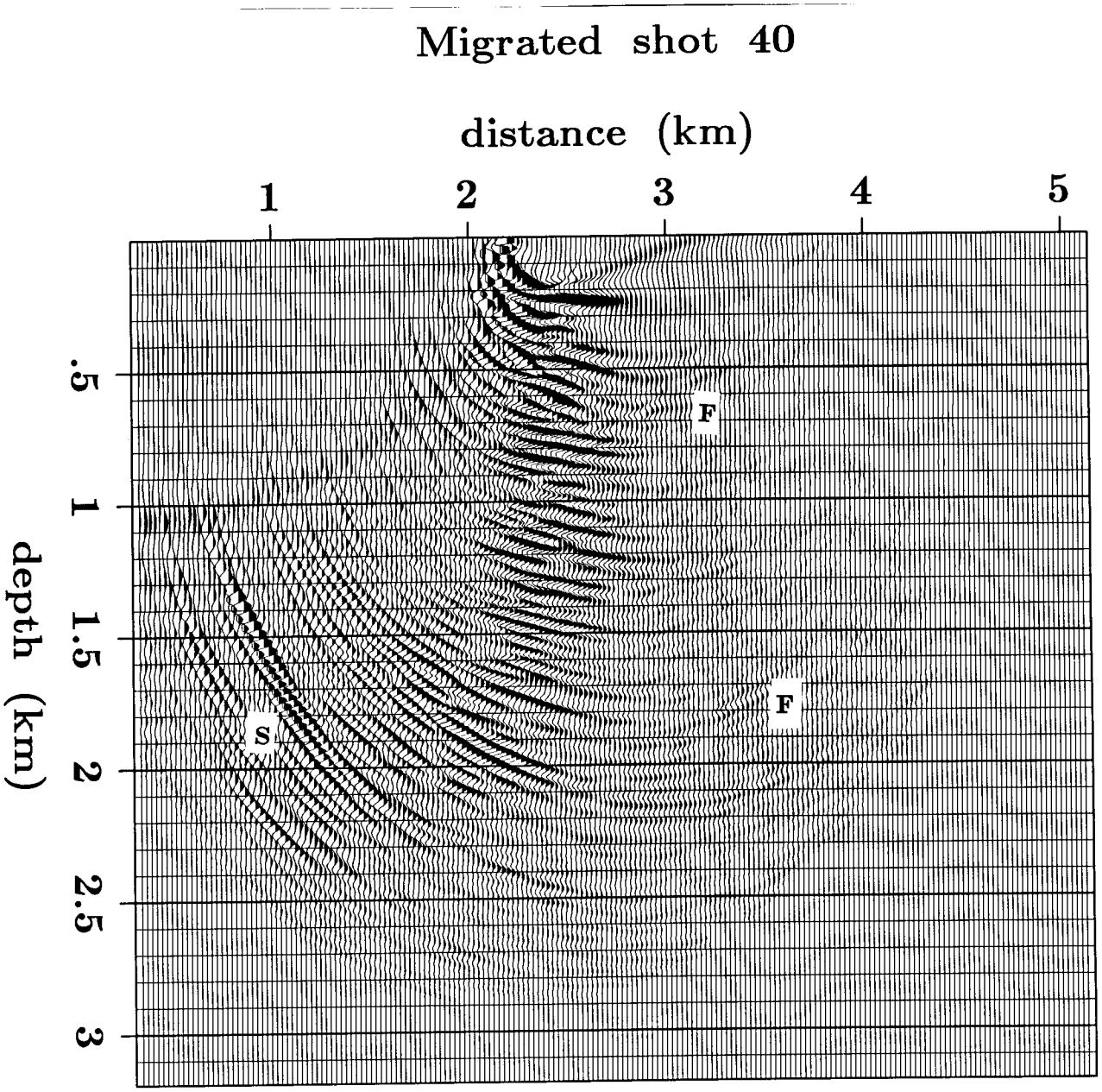

FIG. 11. Prestack migrated profile 40

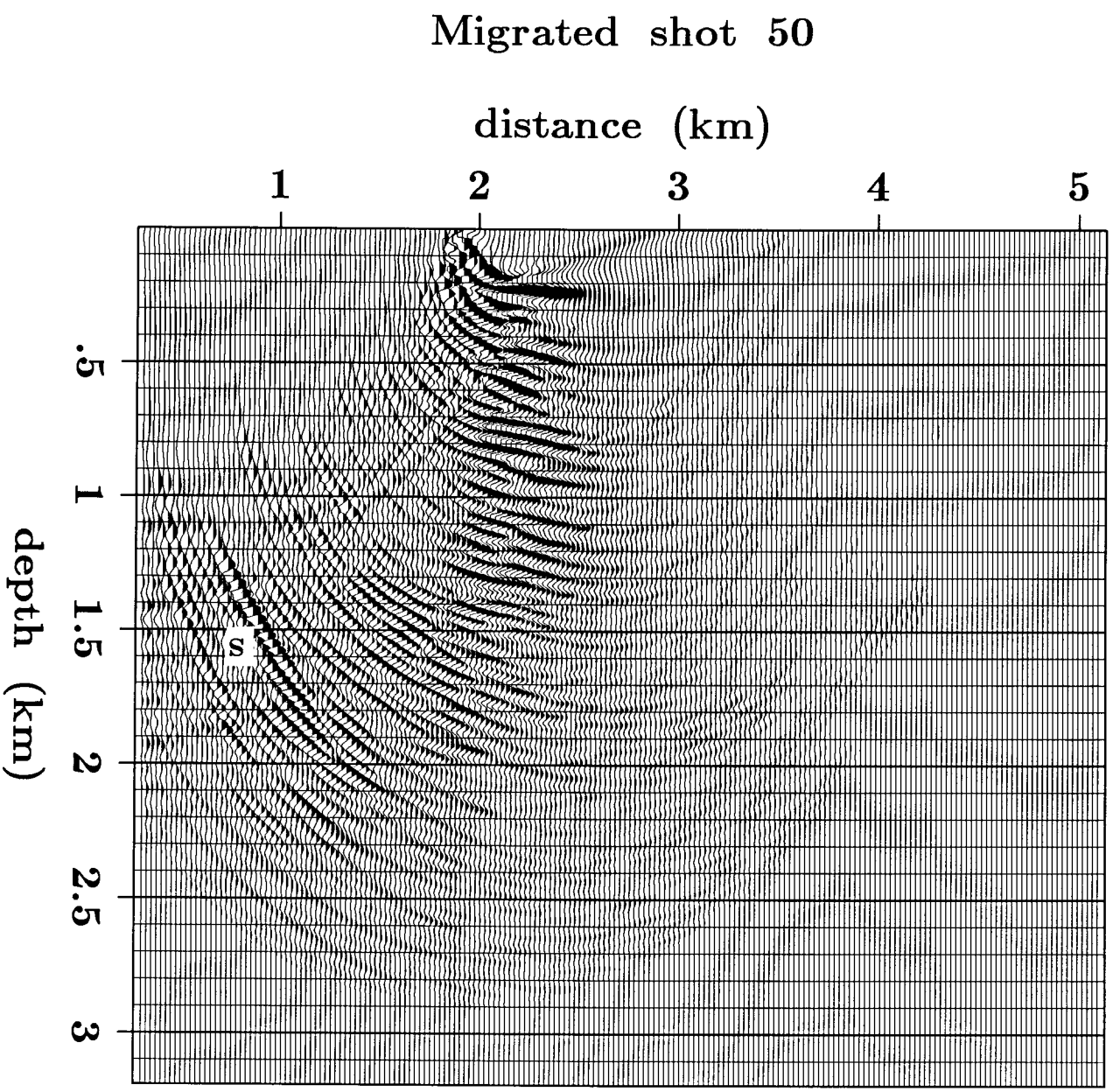

FIG. 12. Prestack migrated profile 50

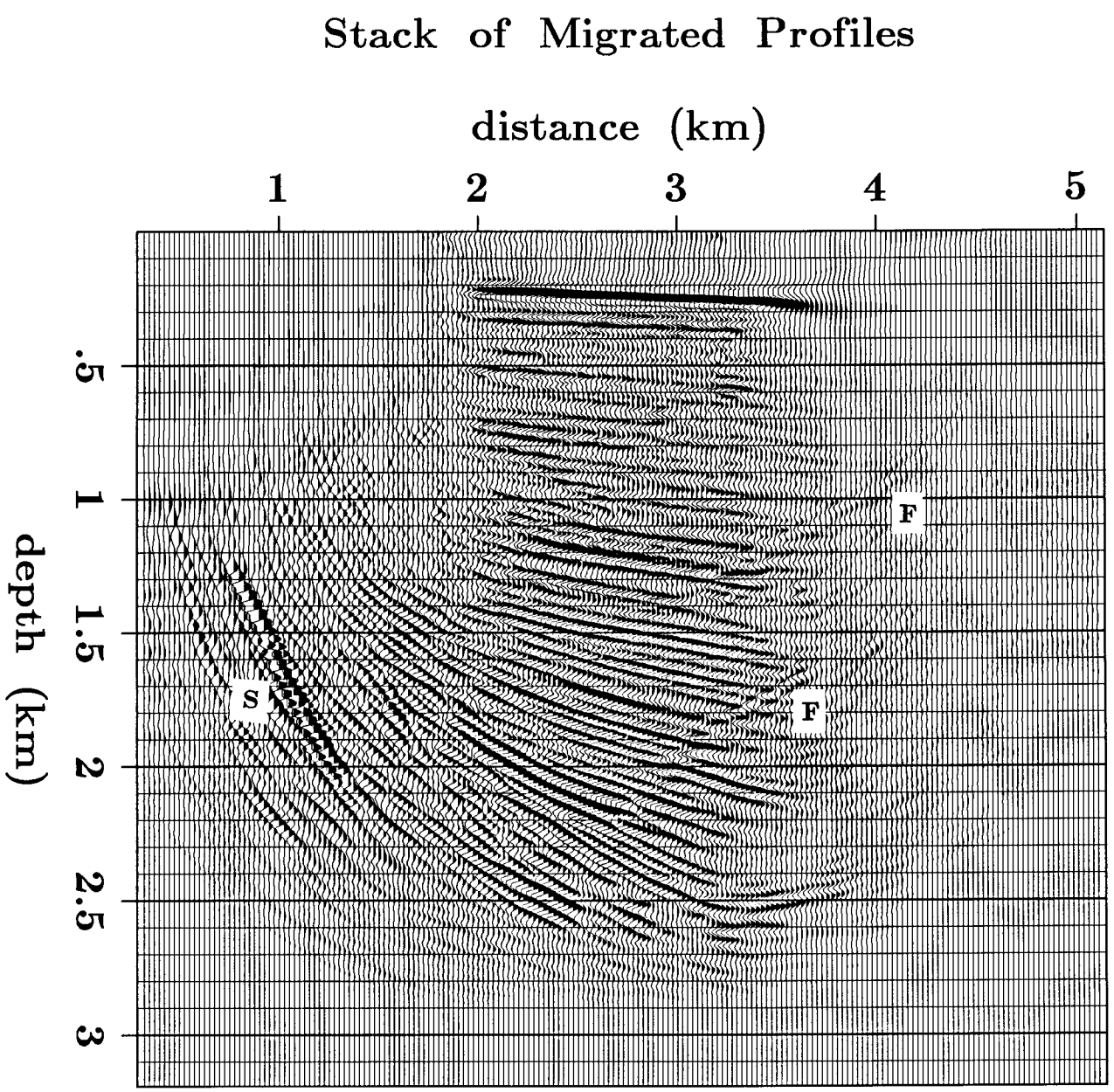

FIG. 13. Stack of 56 prestack migrated profiles. Fault plane "F" and salt interface "S" are well imaged.

stack. Figure 13 is the stack of all 56 profiles that were migrated. The slightly dipping sediments are well imaged in their correct position in depth. The fault plane reflections "F", are evident to the right of the sediments as well as the salt dome-sediment interface "S", on the left side of the image. More profiles need to be migrated to further image the reflectors near the salt interface, as they were only recorded by the last few profiles. Velocity varies only with depth, there was almost no lateral velocity variation evident in the profiles that were migrated, so none was used. As more profiles near the salt dome are migrated, a laterally variable velocity field will probably be needed to get the correct image. Note that the velocities used are interval velocities in depth.

CONCLUSIONS

Reverse time migration provides a simple, physical framework for prestack migration of shot profiles. The method is an accurate depth migration for all dips and velocity variations. Although the method is not computationally cheap, I believe it is competitive with other prestack migration procedures with similar generality. Artifacts caused by the finite extent of the recording geometry are usually not severe, and are easily suppressed by adding images from different shots in their correct locations. The most critical information to the procedure is the velocity model. In areas where conventional methods of imaging work, a first guess at the interval velocities can be obtained through an rms velocity estimate with only slight modification (converted to interval velocity in depth). The method is easily extended to the prestack migration of 3-D profiles provided sufficient memory and computational power are available.

ACKNOWLEDGMENTS

I would like to thank Zhiming Li for allowing me to use his data sets to demonstrate these methods. All of the preliminary work of reading the field tapes through velocity analysis was done by Li, and this saved me a great deal of time and effort. I also thank Pete Mora for use of his depth conversion program and many interesting conversations on finite differences and time reversed propagation of wavefields. Finally thanks go to Chevron for supplying the data set.

REFERENCES

Baysal, E., Kosloff, D.D. and Sherwood, J.W.C., 1984, A two-way non-reflecting wave equation: Geophysics, **49**, 132-141.

Baysal, E., Kosloff, D.D. and Sherwood, J.W.C., 1983, Reverse time migration: Geophysics, **48**, 1514-1524.

Claerbout J. F., 1985, Imaging the earth's interior: Blackwell Scientific Publications., 47-49.

Dablain, M., 1986, The application of high-order differencing to the scalar wave equation: Geophysics, **51**, 54-66.

Etgen, J., 1986, High-order finite-difference reverse time migration with the two-way non-reflecting

wave equation: SEP-48 ,133-146.

Levin, S., 1983, Principle of reverse time migration: SEP-37 ,37-42.

Li, Zhiming, Claerbout, J.F., Ottolini, R.A., 1984, Overturned- wave migration by two-way extrapolation: SEP-38, 141-150.

Whitmore, N.D., 1984, Interactive Depth Migration by Backward time propagation: Presented at the 53rd annual International SEG meeting September 13, 1984, in Las Vegas.

CONVEX 10/1/86

CPU MIN	JOB
40593	Invert2d
31978	fdi1
34805	Prestack
8951	Mvstack
6185	dmand.x
5286	icosfe4
4494	Elastic2d
4452	Mvsdmo
3857	solid
3626	modeld.x
3340	Hdmo
3063	psrtm4.x
2663	Hdmo.ap
2547	Phase
2201	t1d5w
1918	Taplot
1606	Movie
1452	icosfd4
1428	psmig.x
1377	t1d6w
1348	Syn2
1343	t1d5
1331	scdecon
1230	Dmo
1229	icosfe2
1172	t1d6k
1112	sgmig2
1102	Scdecon
1090	Velan
1078	t1d8w
1073	Dw
1038	T15mig
1017	fswem48.x
999	cbinv.x
981	icosfe1
958	Slopro
882	Nmostack
773	Trisp
761	St
757	bombtestk
705	syinmo
681	icosfe5
679	Wiggle
677	Window
632	Dc
611	Invert1d
578	sgmig1
576	ies